

Research Article

Stress Concentration in the Bulk Cr₂O₃: Effects of Temperature and Point Defects

Mazharul M. Islam,^{1,2} Thierry Couvant,³ Philippe Marcus,¹ and Boubakar Diawara¹

¹*Chimie ParisTech, PSL Research University, CNRS, Institut de Recherche de Chimie Paris (IRCP), 11 rue Pierre et Marie Curie, 75005 Paris, France*

²*Mulliken Center for Theoretical Chemistry, Institut für Physikalische und Theoretische Chemie, Universität Bonn, Beringstraße 4–6, 53115 Bonn, Germany*

³*EDF R&D, Centre des Renardières, route de Sens, 77818 Moret-sur-Loing, France*

Correspondence should be addressed to Mazharul M. Islam; rana-islam@thch.uni-bonn.de

Received 12 February 2017; Accepted 4 April 2017; Published 24 April 2017

Academic Editor: Jae Ryang Hahn

Copyright © 2017 Mazharul M. Islam et al. This is an open access article distributed under the Creative Commons Attribution License, which permits unrestricted use, distribution, and reproduction in any medium, provided the original work is properly cited.

Modeling the growth and failure of passive oxide films formed on stainless steels is of general interest for the use of stainless steel as structural material and of special interest in the context of life time extension of light water reactors in nuclear power plants. Using the DFT + U approach, a theoretical investigation on the resistance to failure of the chromium-rich inner oxide layer formed at the surface of chromium-containing austenitic alloys (stainless steel and nickel based alloys) has been performed. The investigations were done for periodic bulk models. The data at the atomic scale were extrapolated by using the Universal Binding Energy Relationships (UBERs) model in order to estimate the mechanical behavior of a 10 μm thick oxide scale. The calculated stress values are in good agreement with experiments. Tensile stress for the bulk chromia was observed. The effects of temperature and structural defects on cracking were investigated. The possibility of cracking intensifies at high temperature compared to 0 K investigations. Higher susceptibility to cracking was observed in presence of defects compared to nondefective oxide, in agreement with experimental observation.

1. Introduction

Chromium-containing iron or nickel based alloys such as stainless steel are chemically protected by surface oxide film (passive film). These passive films are generally rich in chromium oxide [1, 2]. The surface oxide growth and properties play a major role in stress corrosion cracking mechanisms of austenitic alloys (austenitic stainless steels and nickel based alloys) exposed to primary water of pressurized water reactor (PWR). Under operating conditions (aqueous environment, high temperature, residual stress, and eventually neutron irradiation), a complex synergy between the microstructure, the oxidation, and the mechanical load can lead to local cracking [3, 4]. Investigating the growth kinetics of passive layers on stainless steels and their corrosion resistance under different physicochemical and mechanical load is a challenge for improving the lifetime of PWR components [5].

Bulk Cr₂O₃ is an antiferromagnetic insulator which crystallizes in the hexagonal corundum structure (space group *R3c*) [6]. The unit cell contains six formula units where two-thirds of the octahedral sites are occupied by Cr and one-third remains vacant as shown in Figure 1. Both experimental [7–12] and theoretical [13, 14] studies have been performed for the investigation of mechanical properties of Cr₂O₃. Experimental investigations [7, 8] suggest that tensile stresses appear during oxide scale growth controlled by the predominant cationic diffusion, whereas compressive stresses are expected due to oxygen diffusion at grain boundaries. Experimental evaluations indicate a tensile strength within the range 178 to 400 MPa [9–11] and a compressive strength within the range –1.6 GPa to –2.6 GPa [7, 8, 12], both depending on the substrate and oxide layer thicknesses. Very recent DFT + U studies [13, 14] have also evaluated the tensile strength in the bulk chromia ranging from 67.0 to 94.6 GPa along the [0001] direction. It is evident that such calculated

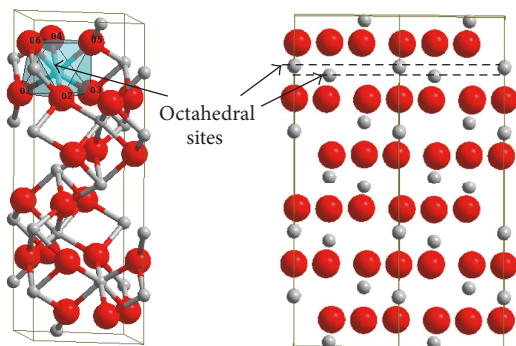


FIGURE 1: Bulk Cr_2O_3 showing the octahedral sites. Red and gray spheres represent oxygen and chromium atoms, respectively.

values seem highly overestimated compared to the experimental values. One of the main reasons is that the quantum chemical DFT calculations were performed at the atomic or nanoscopic scale, whereas the mechanical properties were experimentally measured at a micrometer scale. By applying UBER's model, the authors [13, 14] have demonstrated that the tensile strength for a $10 \mu\text{m}$ thick chromia sample is in the range 380–500 MPa. However, in those studies, other factors affecting the mechanical properties such as temperature and presence of defects were not considered.

The aim of the present study is to compute the resistance to failure of a Cr-rich oxide layer assumed to be composed of chromia (Cr_2O_3). We have performed a theoretical investigation of the mechanical properties associated with the fracture of chromium oxide by adopting the techniques described in a previous investigation [13]. The present study focuses on the DFT calculations of stresses in bulk Cr_2O_3 taking into account the effects of point defects and temperature. The techniques will be utilized for the stress/strain localization in grain boundaries (GBs) of Cr_2O_3 in future study.

2. Methodology

2.1. Tensile Properties. The maximum tensile stress that a material can withstand before failure is known as the tensile strength σ_c . In experimental studies [9–11], tensile properties measurements of oxide layers are performed on macroscopic samples via bending tests where the tensile strength values are estimated from the flexural strength. Typically, this leads to a wide range of values due to various microstructures and presence of defects in the material. The failure of materials is generally initiated through atomic level processes such as bond breaking and dislocation nucleation. DFT calculations provide atomic level insight into these basic processes responsible for the materials' failure.

Total energy calculations were performed within the density functional theory (DFT + U) based on the generalized gradient approximation (GGA) of Perdew and Wang [15]. The Kohn-Sham equations were solved by the Vienna ab initio simulation package (VASP) [16, 17]. VASP code performs an iterative diagonalization of the Kohn-Sham Hamiltonian via unconstrained band-by-band minimization of the norm

of the residual vector to each eigenstate and via optimized charge density mixing routines. The (GGA + U) was used as in [18] in order to describe the strong correlation effects of the oxide. For Cr in Cr_2O_3 , an effective on-site Coulomb interaction parameter $U = 5 \text{ eV}$, was used as defined in our previous investigations [19, 20]. The eigenstates of the electron wave functions are expanded on a plane-wave basis set using pseudopotentials to describe the electron-ion interactions within the projector augmented waves (PAW) approach [21].

The optimization of the atomic geometry at 0 K is performed by determining the exact Hellmann-Feynman forces acting on the ions for each optimization step and by using a conjugate gradient algorithm until the geometric convergence criterion on the energy (0.1 meV/cell or less) is reached. The optimized bulk lattice vectors were calculated to be $a = 5.07 \text{ \AA}$ and $c = 13.85 \text{ \AA}$, very close to experimental values, $a = 4.95 \text{ \AA}$ and $c = 13.57 \text{ \AA}$ [22]. Molecular dynamics calculations at DFT + U level were performed at 300 K.

It is to be noted that the first principles methods perform the tensile strength calculation in nanoscopic samples that yield much overestimated values [13]. The establishment of the Universal Binding Energy Relationships (UBERs) model [23–26] provides an alternative means of extrapolating the results of atomic scale calculations to the longer length scales. Therefore, UBERs model is applied in order to estimate the mechanical behavior of a $10 \mu\text{m}$ thick oxide scale.

2.2. Calculation of Stress. The mechanical properties of chromia are estimated in two ways. The first approach is the “ideal tensile test” which considers uniform elongation of the model (Figure 2(a)) up to failure providing the theoretical tensile strength of the material. This approach is illustrated in Figure 2(b) where the tensile strain ε is operating via a uniaxial and uniform extension of the system with an elongation distance δ (\AA). The second approach considers the formation of a single crack across a specific interatomic plane through the application of tensile load as depicted in Figure 2(c). Combining the two approaches, the resistance to failure of a $10 \mu\text{m}$ thick model can be computed by using the UBERs model as presented in recent theoretical studies [13, 14].

3. Results and Discussion

3.1. Ideal Tensile Test of Bulk Cr_2O_3 . In the simulated tensile test, tensile strain is applied by elongating the system along the direction of the applied load as shown in Figure 2(b). The applied load is directed along the c crystallographic axis ($[0001]$ direction). Thus the axial stress is evaluated for successive elongations. The resulting stress-strain curve (Figure 3(a)) provides a maximum indicating the limit of the resistance to failure of the material. The value of the stress to failure corresponds to the maximum tensile stress (σ_c) that can be experienced by the simulated system. Figure 3(a) shows that the calculated σ_c with the DFT + U method is 57.0 GPa. The maximum strain (δ_c) before fracture is 3.3 \AA . The fracture always occurs perpendicular to the direction of the applied load (as shown in Figure 3(b)). The fracture

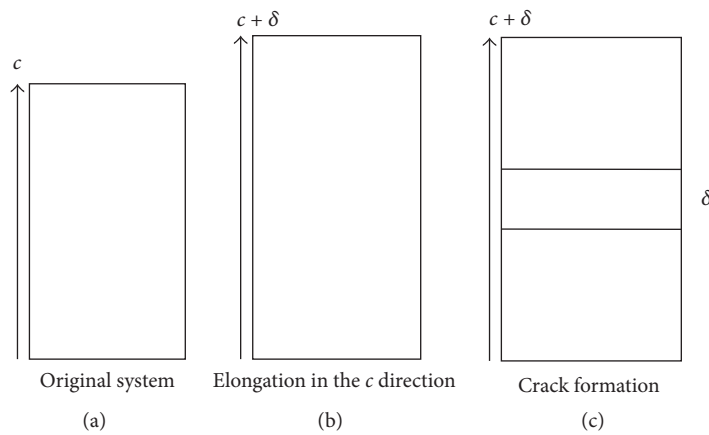


FIGURE 2: Schematic diagrams: (a) the original system showing the lattice parameter c (\AA) along which the load is applied, (b) uniform expansion by a distance δ (\AA) along the direction of the applied load, and (c) insertion of single crack of width δ (\AA).

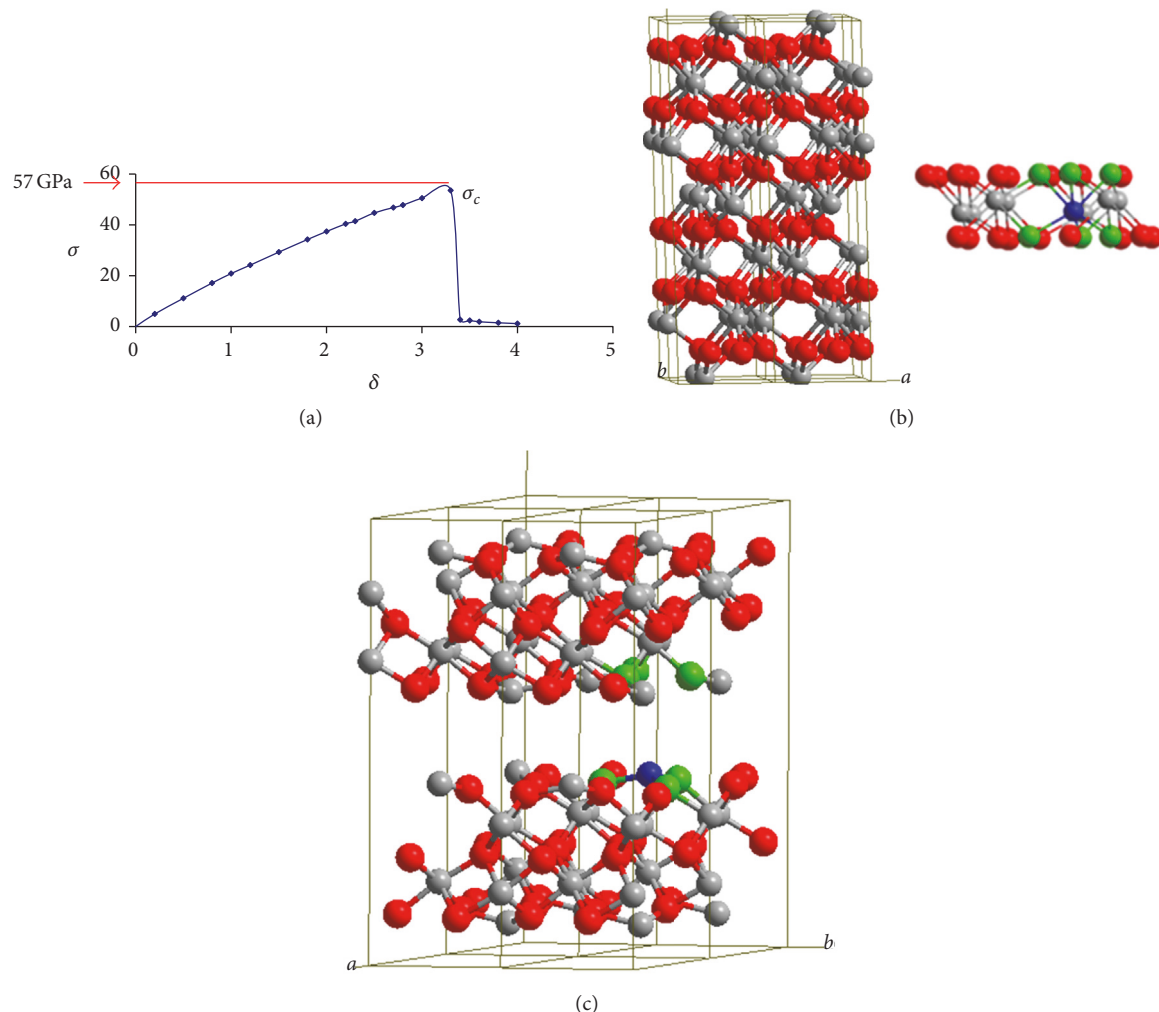


FIGURE 3: (a) Stress σ (GPa) versus strain δ (\AA) curve that provides the ideal tensile test. σ_c is the maximum tensile strength. (b) Crystal structure of Cr_2O_3 bulk, showing position where the fracture happens; (c) Cr_2O_3 bulk system with fracture in the middle. The blue atom corresponds to the specific Cr atom and green atoms are the O forming the octahedron.

TABLE 1: Comparison of calculated δ_c (\AA) and σ_c (GPa) values with the experiment for bulk Cr_2O_3 (the values from the insertion crack tests are in the bracket).

Method	Nondefective			Cr-defective	Experiment [9–11]
	DFT + U	0 K	300 K		
Temperature		1 \times 1 \times 1		UBER	0 K
Supercell		1 \times 1 \times 2	1 \times 1 \times 1		
δ_c	3.3 (1.8)	3.35	1.4	165.70	2.5
σ_c	57.0 (39.9)	54.40	21.5	0.53	22.70
					0.18–0.40

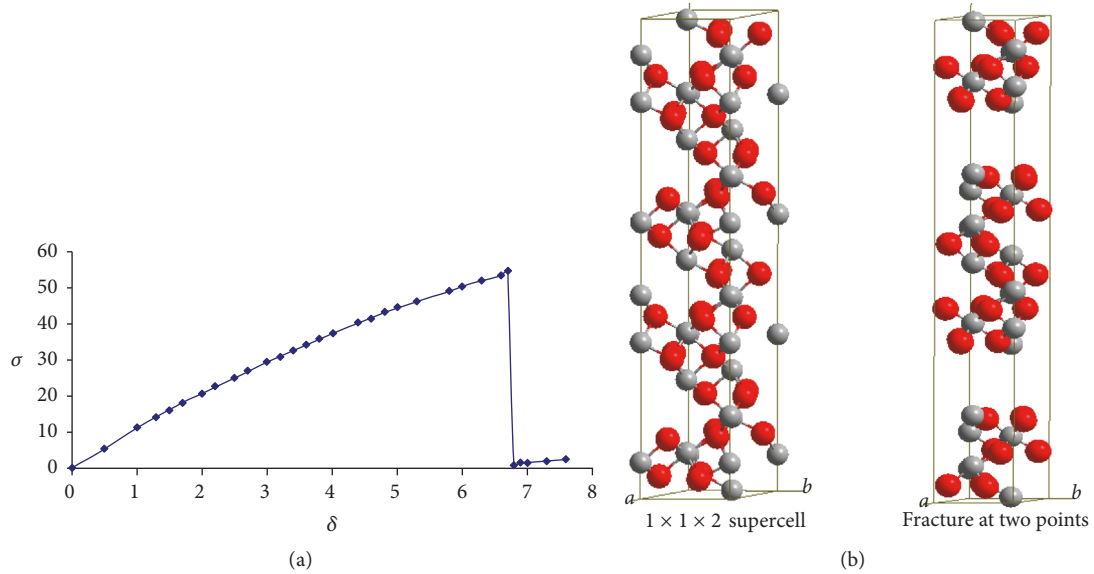


FIGURE 4: Results obtained for a $1 \times 1 \times 2$ supercell of Cr_2O_3 . (a) Stress σ (GPa) versus strain δ (\AA) curve that provides the ideal tensile test. σ_c is the maximum tensile strength. (b) Crystal structure showing the fracture at two points.

appears at the middle of the system, at the upper part of the Cr–O octahedron breaking the three longest bonds (2.048 \AA in the bulk), while the three shorter bonds (1.935 \AA in the bulk) remain. It splits the Cr bilayer in its middle as shown in Figure 3(c).

It appears clearly that the calculated σ_c value is highly overestimated compared to the experimental value (0.18–0.40 GPa [9–11], see Table 1). Although the ideal tensile test is similar to the experimental tensile test conceptually, there is a large discrepancy between the calculated and experimentally measured values of σ_c . We assume that, due to the absence of thermal fluctuations and structural defects, the calculated σ_c is overestimated.

The effect of unit cell size on the calculated properties has been investigated by doubling the unit cell size along the c direction (the direction of applied load). The stress-strain curve is shown in Figure 4(a). The fracture occurs in two planes lying normal to the direction of applied load (Figure 4(b)). The calculated σ_c is 54.40 GPa which is smaller than a $(1 \times 1 \times 1)$ supercell (57.00 GPa , Table 1). This gives an indication that simulation of a very large supercell representing the real system would lower σ_c to a value close to the experimental one. However, due to the limited computer resources, investigation with a larger supercell is out of the scope of the present study. We have also investigated the

effects of temperature and defects on the calculated σ_c , which will be discussed later.

3.2. Strain Localization in Bulk Cr_2O_3 Structure. Strain localization in Cr_2O_3 structure was investigated by the analysis of the structures obtained when elongating the system uniformly along the direction of applied load. The variation of the lengths of the Cr–O bonds around a single Cr atom was determined as a function of the applied tensile strain. As shown in Figure 5(a), there exist three equivalent Cr–O bonds (green) above the Cr atom and another three equivalent Cr–O bonds (blue) below this atom, which is indicated as Cr^* . For comparison, we have adopted same notations as discussed in [13]. The variation of the bond length versus tensile strength curves for Cr–O bonds is plotted in Figure 5(b) where the green curve corresponds to the upper Cr–O bonds and the blue curve corresponds to the lower Cr–O bonds.

It is observed that the Cr–O bond length increases roughly linearly with the applied elongation. The rate of change of bond length is nearly identical for the Cr–O bonds above and below the designated Cr atom until the system fractures. Note that all Cr atoms in Cr_2O_3 are structurally equivalent. Our results suggest that all of the Cr–O bonds in the system accommodate equivalently the tensile load applied along the [0001] crystal direction. After fracture, there is huge

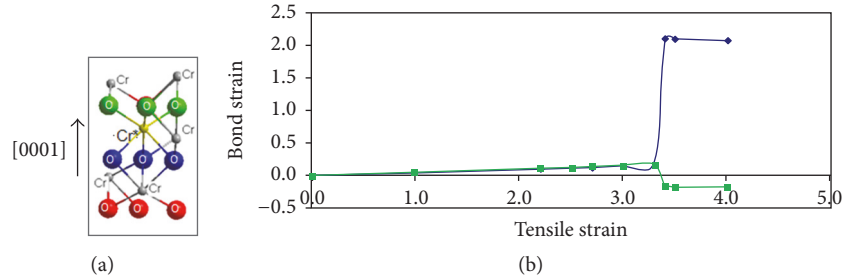


FIGURE 5: (a) Three equivalent Cr–O bonds above and below the Cr atom designated as Cr*. (b) Bond strain versus tensile strain curves for the Cr–O bonds above (green curve) and below (blue curve) the Cr* atom.

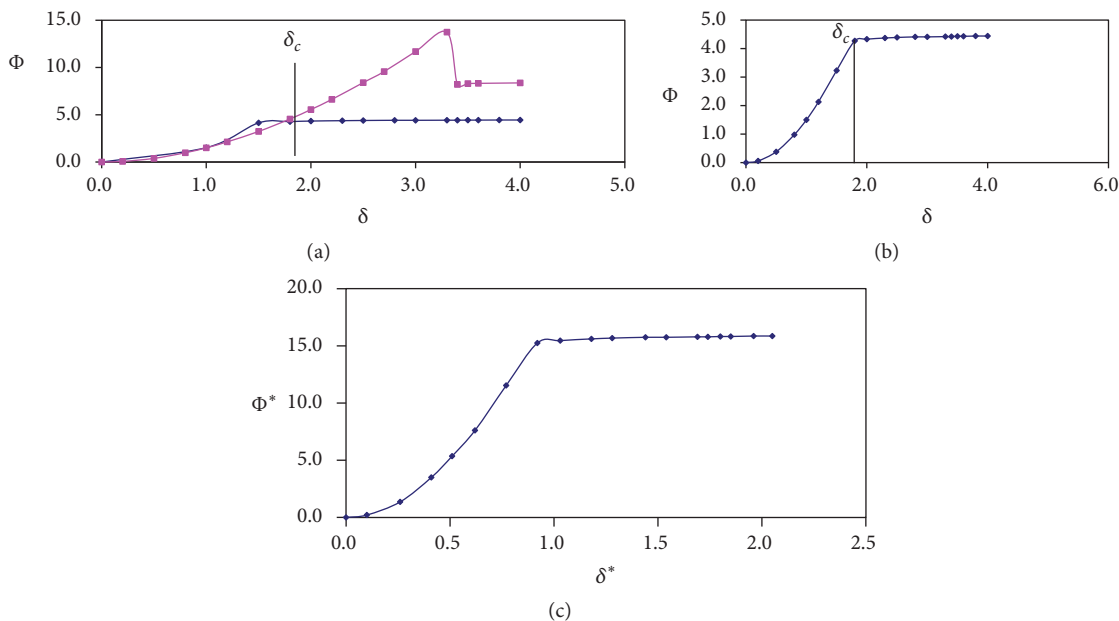


FIGURE 6: Φ (eV) versus δ (\AA) curves: (a) the pink curve corresponds to the uniformly expanded system and the blue curve corresponds to the system with inserted crack, (b) combination of the two series of results from two different limits, and (c) plot of Φ^* versus δ^* providing the UBER curve.

increase in the lower Cr–O bond (as shown in the blue curve of Figure 5(b)), whereas the upper Cr–O bond decreases (as shown in green curve in the Figure 5(b)). These are in good agreement with a previous theoretical study [13].

3.3. UBER Models. Two different limits in which a material can accommodate the applied load can be considered as already depicted in Figure 2. Firstly, the system can accommodate the applied strain (ϵ) by uniform expansion with a distance δ (\AA) along the direction of the applied load. Secondly, the system can accommodate the applied strain (ϵ) by forming a single crack of width δ (\AA).

In both cases, several full optimization calculations were performed for various δ values and the energy Φ of the system is then evaluated for each calculation. The Φ versus δ curves are plotted for both kinds of limit, as shown in Figure 6(a).

For the expanded system, the fracture occurred for $\delta = 3.3 \text{ \AA}$ (pink curve in Figure 6(a)) whereas, for the crack-inserted system, the failure started to operate at lower δ value (below 1.5 \AA , blue curve in Figure 6(a)). For an intermediate

value of $\delta = 1.8 \text{ \AA}$, the energy of the uniformly expanded system was equal to that of the crack-inserted system. This elongation (δ_c) corresponds to the maximum value of δ that the system can experience prior to failure. The combination of the pink and the blue curves leads to Figure 6(b), where δ_c can be evaluated as 1.8 \AA . Evaluating the stress at this point provides an estimate of σ_c .

The renormalization of Φ and δ into the dimensionless quantities can be performed according to following equations:

$$\Phi^* = \frac{\Phi}{2\gamma}, \quad (1)$$

where γ is the surface energy.

$$\delta^* = \frac{\delta_c}{2\sqrt{(N\gamma/C)}}, \quad (2)$$

where N is the number of stoichiometric units and C is the uniaxial elastic constant given by the slope of the plot of $2N\Phi$ versus δ^2 .

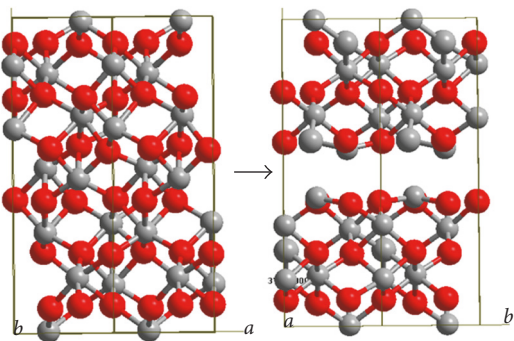


FIGURE 7: Stress calculation in Cr_2O_3 at 300 K. Indication of the position of crack and the structure after cracking.

The curve (Figure 6(c)) obtained by plotting Φ^* versus δ^* is called the UBER; its universality implies that all materials should obey this relationship. More details can be obtained from similar study on Cr_2O_3 [13].

For a 10 μm thick model, $\sigma_c = 0.531 \text{ GPa}$. δ_c is calculated by (2), where δ^* is 1 (maximum of Φ^* versus δ^* curve, Figure 6(c)). The calculated value of δ_c for the 10 μm thick sample is 166 \AA .

The calculated δ_c (\AA) and σ_c (GPa) values are compared with experimental values in Table 1. The experimental σ_c values range from 0.18 to 0.40 GPa. As discussed before, the calculated DFT + U values are much overestimated compared to the experimental value, 57.00 GPa for the uniformly expanded system and 39.90 GPa for the system with inserted crack (the values in the bracket). As indicated by the values of δ_c , the transition between the uniformly expanded and cracked regimes occurs at 1.80 (\AA) when the load is applied along [0001] direction. This can be visualized in the Φ versus δ curve (Figure 6(b)). The transition between the uniformly expanded and cracked regimes is smooth and the curve exhibits the anticipated shape: Φ exhibits an approximately harmonic dependence on δ for small values of δ and asymptotically approaches a constant value as δ tends to infinity. The σ_c value of 0.53 GPa obtained for a 10 μm thick sample using the UBERs model (see Table 1) is in fair agreement with experiments. This shows the ability of the UBER to transform the results of the atomic scale calculations into realistic values of mechanical properties on much longer length scales.

3.4. Effect of Temperature. In reality, experimental measurements of tensile properties are performed at room temperature. In order to simulate the real situation, further investigation was performed at 300 K with the MD simulation. The tensile stress is applied by elongating the system along the direction of the applied load as explained in Figure 2(b). Several MD calculations at 300 K were performed for each of the applied loads. The maximum strain (δ_c) before the fracture is 1.4 \AA for Cr_2O_3 at 300 K which is much smaller than that at 0 K (3.3 \AA). The structures before and after fracture are shown in Figure 7. As at 0 K, the fracture occurs at the midpoint of the Cr bilayer and the resulting Cr half

layers move toward the adjacent O layers. The value of stress at this point along the stress-strain curve (the maximum tensile stress σ_c) is 21.50 GPa. Compared to the experimental value of σ_c , it is observed that the maximum tensile strength is less overestimated at 300 K than that at 0 K (Table 1).

3.5. Cr-Defective Cr_2O_3 . For the Cr-defective Cr_2O_3 , the tensile strain is applied by elongating the system along the direction of the applied load as explained before (see Figure 2(b)). This is done for a series of strains δ and then the stress σ along the direction of the applied load is evaluated for each strain. It is observed that the fracture occurs perpendicular to the applied load axis and the material breaks down near the defect as shown in Figures 8(a) and 8(b).

The resulting stress versus strain curve (Figure 8(c)) provides a maximum indicating the mechanical failure of the material. The value of stress at this point along the stress-strain curve corresponds to the maximum tensile stress (σ_c) that can be sustained by the simulated system. In Figure 8(c), it is observed that the calculated σ_c with the DFT + U method is 22.70 GPa. The maximum strain (δ_c) before fracture is 2.5 \AA . Compared to the experimental value of σ_c , it is observed that the maximum tensile strength is less overestimated in the Cr-defective system than that in the nondefective system (Table 1). This is reasonable as the presence of defect reduces the strain required for creation of fracture or mechanical failure in the system. As all the Cr atoms in Cr_2O_3 are structurally equivalent, the variation of location of defect will not vary the maximum tensile stress and strain of the system. The calculated σ_c and δ_c values will reduce with the reduced concentration of Cr defects in the structure and converge to the experimental values for a very small vacancy concentration. It must be noted that, due to the limited size of the model, one vacancy per unit cell corresponds to a very high vacancy concentration (3.33%).

4. Conclusions

The mechanical properties associated with the fracture of chromia (Cr_2O_3) were evaluated theoretically. The estimation of stress was done by two ways. The first approach considers the effect of subjecting the material to increasing tensile loads until fracture occurs and provides the theoretical tensile strength of the material. The second approach considers the formation of a single crack across a specific interatomic plane through the application of tensile load.

The calculations of the stress related properties were done by using the DFT + U approach applying periodic models. Then the atomic level results were extrapolated by using the UBERs model in order to obtain a realistic estimate for a 10 μm thick sample. Our investigation shows also that the temperature and the presence of point defects play important role for the mechanical properties associated with fracture. It was observed that stress for the bulk chromia is tensile. These are in good agreement with experimental observations. Investigations are ongoing to understand the stress/strain localization in the grain boundaries of chromium oxides by applying the above-mentioned techniques and methods.

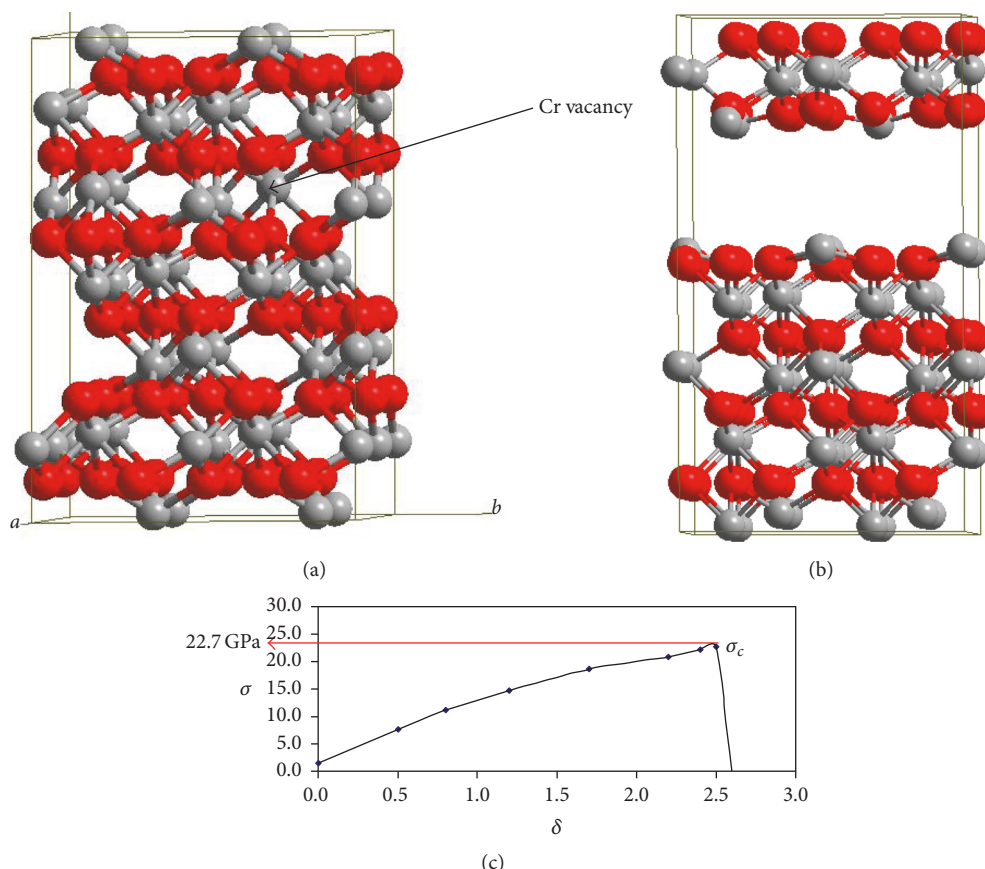


FIGURE 8: Stress calculation in the Cr-defective Cr_2O_3 . (a) The arrow indicates the position of the Cr vacancy (Cr V), (b) fracture initiates at the position of the vacancy (c) stress σ versus strain δ plot for the Cr-defective system. σ_c is the maximum tensile strength.

Conflicts of Interest

The authors declare that there are no conflicts of interest regarding the publication of this paper.

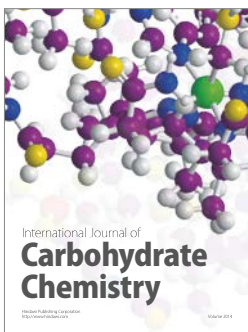
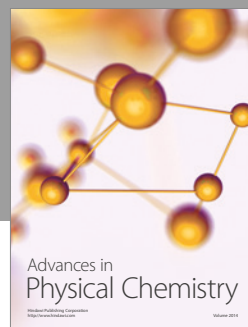
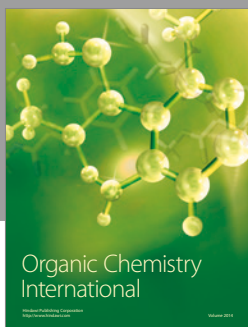
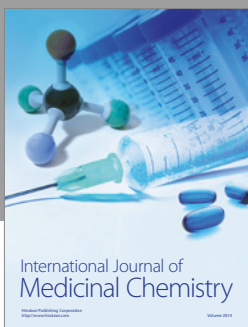
Acknowledgments

A postdoctoral grant of the Electricite de France (EDF) for the support of Mazharul M. Islam is acknowledged.

References

- [1] A. Machet, A. Galtayries, S. Zanna et al., "XPS and STM study of the growth and structure of passive films in high temperature water on a nickel-base alloy," *Electrochimica Acta*, vol. 49, no. 22–23, pp. 3957–3964, 2004.
- [2] V. Maurice, W. P. Yang, and P. Marcus, "X-Ray photoelectron spectroscopy and scanning tunneling microscopy study of passive films formed on (100) Fe-18Cr-13Ni single-crystal surfaces," *Journal of The Electrochemical Society*, vol. 145, pp. 909–920, 1998.
- [3] P. Scott, "A review of irradiation assisted stress corrosion cracking," *Journal of Nuclear Materials*, vol. 211, pp. 101–122, 1994.
- [4] W. I. Clarke and G. M. Gordon, "Investigation of stress corrosion cracking susceptibility of Fe-Ni-Cr alloys in nuclear reactor water environments," *Corrosion*, vol. 29, pp. 1–12, 1973.
- [5] B. Diawara, Y.-A. Beh, and P. Marcus, "Nucleation and growth of oxide layers on stainless steels (FeCr) using a virtual oxide layer model," *Journal of Physical Chemistry C*, vol. 114, no. 45, pp. 19299–19307, 2010.
- [6] L. Pauling and S. B. Hendricks, "The crystal structures of hematite and corundum," *Journal of the American Chemical Society*, vol. 47, no. 3, pp. 781–790, 1925.
- [7] A. M. Huntz, "Stresses in NiO , Cr_2O_3 and Al_2O_3 oxide scales," *Materials Science and Engineering: A*, vol. 201, pp. 211–228, 1995.
- [8] A. M. Huntz, A. Piant, J. L. Lebrun, and S. Daghig, "Evidence of stress relaxation in thermally grown oxide layers—experiments and modelling," *Materials Science and Engineering: A*, vol. 248, pp. 44–55, 1998.
- [9] Y. Takano, T. Komeda, M. Yoshinaka, K. Hirota, and O. Yamaguchi, "Fabrication, microstructure, and mechanical properties of $\text{Cr}_2\text{O}_3/\text{ZrO}_2(2.5\text{Y})$ composite ceramics in the Cr_2O_3 -rich region," *Journal of the American Ceramic Society*, vol. 81, no. 9, pp. 2497–2500, 1998.
- [10] T. Li, R. J. Brook, and B. Derby, "Fabrication of reaction-bonded Cr_2O_3 ceramics," *Journal of the European Ceramic Society*, vol. 19, no. 8, pp. 1651–1664, 1999.
- [11] K. Hirota, H. Motono, M. Yoshinaka, and O. Yamaguchi, "Fabrication and mechanical properties of almost fully-densified Cr_2O_3 ceramics," *Journal of Materials Science Letters*, vol. 21, no. 11, pp. 853–854, 2002.
- [12] M. Kemdehounja, J. L. Grosseau-Poussard, and J. F. Dinhut, "Substrate grain boundary effect on residual stress distribution

- at micrometer scale in chromia oxide thin films," *Applied Physics Letters*, vol. 92, Article ID 241924, 4 pages, 2008.
- [13] N. J. Mosey and E. A. Carter, "Ab initio LDA+U prediction of the tensile properties of chromia across multiple length scales," *Journal of the Mechanics and Physics of Solids*, vol. 57, no. 2, pp. 287–304, 2009.
 - [14] N. J. Mosey and E. A. Carter, "Shear strength of chromia across multiple length scales: an LDA + U study," *Acta Materialia*, vol. 57, no. 10, pp. 2933–2943, 2009.
 - [15] J. P. Perdew and Y. Wang, "Accurate and simple analytic representation of the electron-gas correlation energy," *Physical Review B*, vol. 45, no. 23, pp. 13244–13249, 1992.
 - [16] G. Kresse and J. Hafner, "Ab initio molecular-dynamics simulation of the liquid-metal-amorphous-semiconductor transition in germanium," *Physical Review B*, vol. 49, no. 20, pp. 14251–14269, 1994.
 - [17] G. Kresse and J. Furthmüller, "Efficiency of ab-initio total energy calculations for metals and semiconductors using a plane-wave basis set," *Computational Materials Science*, vol. 6, no. 1, pp. 15–50, 1996.
 - [18] A. Rohrbach, J. Hafner, and G. Kresse, "Ab initio study of the (0001) surfaces of hematite and chromia: Influence of strong electronic correlations," *Physical Review B*, vol. 70, Article ID 125426, pp. 1–17, 2004.
 - [19] A. G. Van Der Geest, M. M. Islam, T. Couvant, and B. Diawara, "Energy ordering of grain boundaries in Cr₂O₃: insights from theory," *Journal of Physics Condensed Matter*, vol. 25, no. 48, Article ID 485005, 9 pages, 2013.
 - [20] F. Lebreau, M. M. Islam, B. Diawara, and P. Marcus, "Structural, magnetic, electronic, defect, and diffusion properties of Cr₂O₃: a DFT+ U study," *Journal of Physical Chemistry C*, vol. 118, no. 31, pp. 18133–18145, 2014.
 - [21] G. Kresse and D. Joubert, "From ultrasoft pseudopotentials to the projector augmented-wave method," *Physical Review B*, vol. 59, pp. 1758–1775, 1999.
 - [22] L. W. Finger and R. M. Hazen, "Crystal structure and isothermal compression of Fe₂O₃, Cr₂O₃, and V₂O₃ to 50 kbars," *Journal of Applied Physics*, vol. 51, no. 10, pp. 5362–5367, 1980.
 - [23] J. H. Rose, J. R. Smith, and J. Ferrante, "Universal features of bonding in metals," *Physical Review B*, vol. 28, no. 4, pp. 1835–1845, 1983.
 - [24] T. Hong, J. R. Smith, D. J. Srolovitz, J. G. Gay, and R. Richter, "Determining ab initio interfacial energetics," *Physical Review B*, vol. 45, no. 15, pp. 8775–8778, 1992.
 - [25] O. Nguyen and M. Ortiz, "Coarse-graining and renormalization of atomistic binding relations and universal macroscopic cohesive behavior," *Journal of the Mechanics and Physics of Solids*, vol. 50, no. 8, pp. 1727–1741, 2002.
 - [26] R. L. Hayes, M. Ortiz, and E. A. Carter, "Universal binding-energy relation for crystals that accounts for surface relaxation," *Physical Review B—Condensed Matter and Materials Physics*, vol. 69, no. 17, Article ID 172104, 4 pages, 2004.



Hindawi

Submit your manuscripts at
<https://www.hindawi.com>

